International Journal of Fracture **78:** 227–239, 1996.
© 1996 *Kluwer Academic Publishers. Printed in the Netherlands.*

A unified model for dislocation nucleation, dislocation emission and dislocation free zone*

T.C. WANG, K.R. WANG and Y.W. ZHANG
LNM, Institute of Mechanics, Chinese Academy of Sciences, Beijing 100080, Peoples Republic of China

Received 5 December 1994; accepted in revised form 10 November 1995

Abstract. In this paper, a unified model for dislocation nucleation, emission and dislocation free zone is proposed based on the Peierls framework. Three regions are identified ahead of the crack tip. The emitted dislocations, located away from the crack tip in the form of an inverse pileup, define the plastic zone. Between that zone and the cohesive zone immediately ahead of the crack tip, there is a dislocation free zone. With the stress field and the dislocation density field in the cohesive zone and plastic zone being, respectively, expressed in the first and second Chebyshev polynomial series, and the opening and slip displacements in trigonometric series, a set of nonlinear algebraic equations can be obtained and solved with the Newton-Raphson Method. The results of calculations for pure shearing and combined tension and shear loading after dislocation emission are given in detail. An approximate treatment of the dynamic effects of the dislocation emission is also developed in this paper, and the calculation results are in good agreement with those of molecular dynamics simulations.

1. Introduction

This paper is concerned with the dislocation behavior near a crack tip. The process of dislocation emission form a stressed crack has been observed in numerous experiments [1, 2, 3]. As pointed out by Ohr [1], a dislocation will be generated at the crack tip if the applied stress is sufficiently large. Once generated, the dislocation will move out of the crack tip area, leaving behind a dislocation free zone. In their pioneering work, Rice and Thomson [4] presented a dislocation emission model to characterize the plastic shear at a crack tip and developed a quantitative criterion for ductile versus brittle behavior.

Recently Rice [5], Schoeck [6], Rice et al. [7] and Beltz and Rice [8] have reanalyzed the Rice-Thomson criterion on the basis of the Peierls model. For the mode II case, Rice [5] presented an exact solution for the loading at the nucleation instability and identified a solid-state parameter, the unstable stacking energy γ_{us}, which characterizes the resistance to dislocation nucleation.

A new approach was developed by Wang [9] with a slightly modified Rice concept. Both the dislocation nucleation and emission from the crack tip were analyzed based on Peierls framework. The calculation clearly shows that there is a well-defined region of fairly 'perfect' crystal between the emitted dislocation and the crack tip area, which can be treated as the dislocation free zone. But that approach proposed by Wang [9] is only valid for the situation where the emitted dislocation is not far away from the crack tip.

This paper is a continuation of the work of [9], where a unified model of dislocation nucleation, emission and dislocation free zone is developed. An approximate approach is

* Presented at the Far East Fracture Group (FEFG) International Symposium on Fracture and Strength of Solids, 4–7 July 1994 in Xi'an, China.

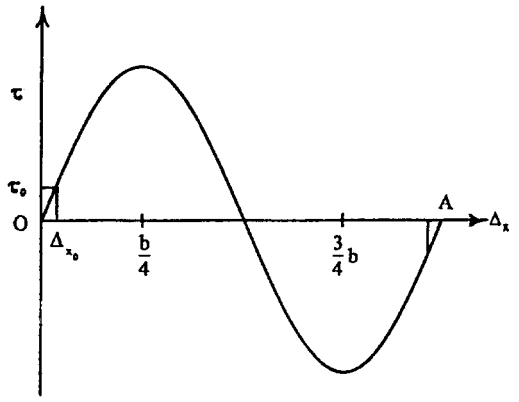

Figure 1. Shear stress versus shear displacement on a slip plane.

also developed which takes into account the dynamic effect of the dislocation emission. The calculation results agree well with those of molecular dynamics simulations.

2. The description of the model

Suppose that the crack front is contained within one of the possible slip planes in a crystal. For a general loading, Beltz and Rice [7] proposed a generalized constitutive relation*

$$\begin{cases} \tau_x = \tau_{\max} A(\Delta_y) \sin\left(2\pi \dfrac{\Delta_x}{b}\right), \\ \sigma_y = \sigma_{\max} B(\Delta_x) \dfrac{\Delta_y}{L} e^{1-(\Delta_y/L)}, \end{cases} \tag{1}$$

where

$$A(\Delta_y) = \left(1 + \frac{\Delta_y}{L}\right) e^{-(\Delta_y/L)}, \tag{2}$$

$$B(\Delta_x) = 1 - q \sin^2\left(\pi \frac{\Delta_x}{b}\right), \qquad q = \frac{\gamma_{us}}{2\gamma_s}, \tag{3}$$

where γ_s is the surface energy, γ_{us} the unstable stacking energy, and L is the scaling length of the Thomas–Fermi screening length [10].

As shown in Figure 1, Δ_x denotes the relative displacement of two atomic planes adjacent to the slip plane. With δ_x defined as the slip displacement discontinuity on a mathematical cut coincident with the slip plane, we have

$$\Delta_x = \delta_x + \frac{\tau}{\mu} h, \tag{4}$$

where h is the interplanar spacing.

* Only the case of $r = 0$ is considered here.

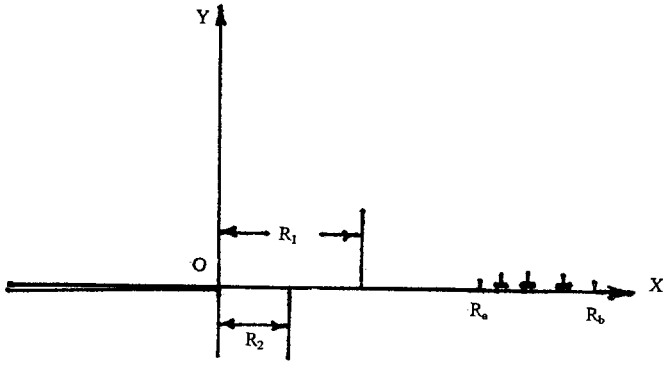

Figure 2. Cohesive zone, decohesive zone ahead of a crack tip, dislocation free zone and emitted dislocations.

δ_x can be taken as the plastic shearing along the slip plane. According to the crystal plasticity given by Hill [11], Asaro [12] among others, there will be no plastic shearing until the resolved shear stress τ reaches the critical shear stress τ_0. Hence (4) becomes

$$\Delta_x = \begin{cases} \delta_x + \dfrac{\tau_x}{\mu} h, & \tau_x > \tau_0, \\ \dfrac{\tau_x}{\mu} h, & \tau_x \leqslant \tau_0. \end{cases} \tag{5}$$

Let Δ_y denote the relative atomic separation across the slip plane, which can similarly be expressed as

$$\Delta_y = \begin{cases} \delta_y + \dfrac{\sigma_y}{E} h, & \sigma_y > \sigma_0, \\ \dfrac{\sigma_y}{E} h, & \sigma_y \leqslant \sigma_0, \end{cases} \tag{6}$$

where δ_y is the opening displacement discontinuity on the slip plane, σ_0 the yield stress, and E the Young's modulus of the crystal.

Figure 2 shows a plane strain or plane stress semi-infinite crack, which lies on the negative x-axis with its tip at $x = 0$. Let R_1 denote the length of the cohesive zone for the slip displacement and R_2 the length of the decohesive zone for the opening displacement. Beyond R_1, there is no discontinuity for the slip displacement, and beyond R_2, discontinuity of the opening displacement vanishes.

The emitted dislocations are located at positions x_i $(i = 1, 2, \ldots, N_0)$ within the interval (R_a, R_b) characterizing the plastic zone formed by the emitted dislocations. The interval (R_2, R_a) can be treated as the dislocation free zone.

3. Basic formulas

According to Wang [9] and Loo [13], the traction on the cohesive zone ahead of the crack tip is

$$\sigma_y - i\tau_{xy} = \sigma_y^{(0)} - i\tau_{xy}^{(0)} + \frac{2\mu}{(\kappa+1)\pi i} \int_0^{R_b} \frac{\sqrt{\tau}\,\hat{b}(\tau)}{\sqrt{x}\,(x-\tau)}\,\mathrm{d}\tau, \tag{7}$$

where $\sigma_y^{(0)}, \tau_{xy}^{(0)}$ are the singular stress field, and $\hat{b}(\tau) = b_x(\tau) + ib_y(\tau)$.

Equation (7) can be represented as

$$\frac{2\mu}{(\kappa+1)\pi}\left\{\int_0^{R_1} + \int_{R_a}^{R_b}\right\}\frac{\sqrt{\tau}\, b_x(\tau)}{x-\tau}\,\mathrm{d}\tau = \sqrt{x}\,[\tau_{xy} - \tau_{xy}^{(0)}], \tag{8a}$$

$$\frac{2\mu}{(\kappa+1)\pi}\int_0^{R_2}\frac{\sqrt{\tau}\, b_y(\tau)}{x-\tau}\,\mathrm{d}\tau = \sqrt{x}\,[\sigma_y - \sigma_y^{(0)}]. \tag{8b}$$

Introduce the following nondimensional quantities

$$t_1 = \frac{x}{R_1}, \qquad t_2 = \frac{x}{R_2}, \qquad s_1 = \frac{\tau}{R_1},$$
$$s_2 = \frac{\tau}{R_2}, \qquad t = \frac{x}{R_b}, \qquad \tau = \frac{\tau}{R_b},$$

and let

$$\begin{cases} F_1(t_1) = \sqrt{t_1}\, b_x(x)\cdot\dfrac{\mu}{\kappa+1}, \\ g_1(t_1) = \sqrt{t_1}\,[\tau_{xy} - \tau_{xy}^{(0)}], \end{cases} \tag{9}$$

$$\begin{cases} F_2(t_2) = \sqrt{t_2}\, b_y(x)\dfrac{\mu}{\kappa+1}, \\ g_2(t_2) = \sqrt{t_2}\,[\sigma_y - \sigma_y^{(0)}], \end{cases} \tag{10}$$

$$F(t) = \sqrt{t}\, b_x(x)\frac{\mu}{(\kappa+1)}. \tag{11}$$

Then (8) becomes

$$\begin{cases} -\dfrac{2}{\pi}\left\{\displaystyle\int_0^1 \frac{F_1(s_1)\,\mathrm{d}s_1}{s_1 - t_1} + \sqrt{\frac{R_b}{R_1}}\int_\rho^1 \frac{F(s)\,\mathrm{d}s}{s-t}\right\} = g_1(t_1), \\ -\dfrac{2}{\pi}\displaystyle\int_0^1 \frac{F_2(s_2)\,\mathrm{d}s_2}{s_2 - t_2} = g_2(t_2), \end{cases} \tag{12}$$

where

$$\rho = \frac{R_a}{R_b}.$$

The singularity of the dislocation density $\hat{b}(x)$ is less than $1/\sqrt{x}$ at the crack tip, while the dislocation density $\hat{b}(x)$ vanishes at the end of the cohesive zone.

With the variable translations: $t_1 = \frac{1}{2}(1+\cos\theta), t_2 = \frac{1}{2}(1+\cos\varphi)$ and $t = \rho + \frac{1}{2}(1-\rho)(1+\cos\psi)$, functions $F_1(t_1), F_2(t_2)$ and $F(t)$ can be expressed as the following sine series

$$\begin{cases} F_1(t_1) = \dfrac{1}{2}\displaystyle\sum_{m=1}^{\infty}\alpha_m \sin m\theta, \qquad t_1 = \tfrac{1}{2}(1+\cos\theta) \quad 0 \leqslant \theta \leqslant \pi, \\ F_2(t_2) = \dfrac{1}{2}\displaystyle\sum_{m=1}^{\infty}\beta_m \sin m\varphi, \qquad t_2 = \tfrac{1}{2}(1+\cos\varphi) \quad 0 \leqslant \varphi \leqslant \pi, \\ F(t) = \dfrac{1}{2}\displaystyle\sum_{m=1}^{\infty}\gamma_m \sin m\psi, \quad 0 \leqslant \psi \leqslant \pi. \end{cases} \tag{13}$$

Equation (13) can be rewritten as

$$\begin{cases} F_1(t_1) = \frac{1}{2}\sqrt{1-\eta_1^2} \cdot \sum_{m=1}^{\infty} \alpha_m U_m(\eta_1), \\ F_2(t_2) = \frac{1}{2}\sqrt{1-\eta_2^2} \cdot \sum_{m=1}^{\infty} \beta_m U_m(\eta_2), \\ F(t) = \frac{1}{2}\sqrt{1-\eta^2} \sum_{m=1}^{\infty} \gamma_m U_m(\eta), \end{cases} \tag{14}$$

where $U_m(\eta)$ is the second Chebyshev polynomial

$$U_m(\eta) = \frac{\sin m\theta}{\sin\theta}, \qquad \eta = \cos\theta, \quad m = 1, 2, \ldots.$$

Substituting (14) into (13) and using the following formula [16]

$$\frac{1}{\pi}\int_{-1}^{1} \frac{\sqrt{1-\xi^2}\, U_m(\xi)\, \mathrm{d}\xi}{\xi - \eta} = -T_m(\eta), \tag{15}$$

$$T_m(\eta) = \begin{cases} \cos m\theta, & \eta = \cos\theta, \quad -1 \leqslant \eta \leqslant 1, \\ [\eta - \sqrt{\eta^2 - 1}]^m, & \eta > 1, \\ [\eta + \sqrt{\eta^2 - 1}]^m, & \eta < -1, \end{cases}$$

one obtains

$$\begin{cases} g_1(t_1) = \sum_{m=1}^{\infty} \alpha_m T_m(\eta_1) + \sqrt{\frac{R_b}{R_1}} \sum_{m=1}^{\infty} \gamma_m T_m(\eta), \\ g_2(t_2) = \sum_{m=1}^{\infty} \beta_m T_m(\eta_2), \end{cases} \tag{16}$$

where $T_m(\eta)$ is the generalized first Chebyshev polynomial.

The opening displacement and sliding displacement take the form

$$\delta_x + i\delta_y = \int_x^{R_b} \hat{b}(\tau)\, \mathrm{d}\tau. \tag{17}$$

Using (11) and (15), we obtain

$$\frac{\mu}{(\kappa+1)}\delta_x = (1-\rho)\frac{R_b}{4} \cdot \sum_{m=1}^{\infty} \gamma_m W_m(\psi), \quad R_a \leqslant x \leqslant R_b, \tag{18}$$

$$\frac{\mu}{(\kappa+1)}\delta_x = \frac{R_1}{4} \sum_{m=1}^{\infty} \alpha_m V_m(\theta) + \frac{\mu}{(\kappa+1)} N_0 b, \quad 0 \leqslant x \leqslant R_1, \tag{19}$$

where

$$W_m(\psi) = \int_0^{\psi} \frac{\sin m\theta \sin\theta \, \mathrm{d}\theta}{\sqrt{\rho + \frac{1}{2}(1-\rho)(1+\cos\theta)}},$$

$$\frac{\mu}{(\kappa+1)}\delta_y = \frac{R_2}{4}\sum_{m=1}^{\infty}\beta_m V_m(\varphi), \quad 0 \leqslant x \leqslant R_2, \tag{20}$$

$$V_m(\theta) = \frac{\sin(m-\frac{1}{2})\theta}{m-\frac{1}{2}} - \frac{\sin(m+\frac{1}{2})\theta}{m+\frac{1}{2}}, \tag{21}$$

where b is the magnitude of Burgers vector, N_0 the number of emitted dislocations.

The singular stress field can be expressed as

$$\sigma_y^{(0)} + i\tau_{xy}^{(0)} = \frac{K}{\sqrt{2\pi r}}. \tag{22}$$

Here $K = K_{\mathrm{I}} + iK_{\mathrm{II}}$ is the complex stress intensity factor.

Substituting (22) into (11) and (12), we obtain

$$\begin{cases} \tau_{xy} = \dfrac{1}{\sqrt{t_1}}\left[g_1(t_1) + \dfrac{K_{\mathrm{II}}}{\sqrt{2\pi R_1}}\right], \\ \sigma_y = \dfrac{1}{\sqrt{t_2}}\left[g_2(t_2) + \dfrac{K_{\mathrm{I}}}{\sqrt{2\pi R_2}}\right]. \end{cases} \tag{23}$$

The Barenblatt's formula can be expressed as

$$\begin{cases} \dfrac{K_{\mathrm{II}}}{\sqrt{2\pi R_1}} = \dfrac{1}{\pi}\displaystyle\int_0^{\pi}\left[\sqrt{t_1}\,\tau_{xy} - \sqrt{\frac{R_b}{R_1}}\sum_{m=1}^{\infty}\gamma_m T_m(\eta)\right]\mathrm{d}\theta, \\ \dfrac{K_{\mathrm{I}}}{\sqrt{2\pi R_2}} = \dfrac{1}{\pi}\displaystyle\int_0^{\pi}\sqrt{t_2}\,\sigma_y\,\mathrm{d}\varphi = \frac{1}{\pi\sqrt{R_2}}\int_0^{R_2}\frac{\sigma_y}{\sqrt{R_2 - x}}\,\mathrm{d}x. \end{cases} \tag{24}$$

Formulas (13), (16)–(20) and (23), (24) are the basic formulas of this paper.

4. Calculation methods and results

The unknown coefficients $\{\alpha_m\}$, $\{\beta_m\}$ and $\{\gamma_m\}$ are chosen as the basic unknown quantities. The infinite series in (13) and (16) can be approximated with a sufficient degree of accuracy by the corresponding truncated series.

The cohesive zone $0 \leqslant x \leqslant R_1$ is discretized into M elements, which vary in size along the region. The nodal points are given by the following expression

$$x_i = \tfrac{1}{2}R_1\left[1 + \cos\left(\frac{(i-1)\pi}{M}\right)\right]. \tag{25}$$

Similarly the decohesive zone $0 \leqslant x \leqslant R_2$ is divided into N elements. The nodal points are given by the formula

$$x_j = \tfrac{1}{2}R_2\left[1 + \cos\left(\frac{(j-1)\pi}{N}\right)\right]. \tag{26}$$

The influence zone of the emitted dislocations $R_a \leqslant x \leqslant R_b$ is discretized into M_* elements and the nodal points are

$$x_k = R_b \left\{ \rho + \tfrac{1}{2}(1-\rho)\left[1 + \cos\left(\frac{(k-1)\pi}{M_*}\right)\right]\right\}. \tag{27}$$

The governing equations are then transformed into a set of nonlinear algebraic equations.

$$\begin{cases} \displaystyle\sum_{k=1}^{M} a_{ik}\alpha_k + \sum_{k=1}^{M_*} b_{ik}\gamma_k - \tau_{\max} A(\Delta_{yi}) \sin\left(2\pi \frac{\Delta_{xi}}{b}\right) = 0, \quad i = 1, 2, \ldots, M, \\ \displaystyle\sum_{k=1}^{N} b'_{jk}\beta_k - \sigma_{\max} B(\Delta'_{xj}) \frac{\Delta'_{yj}}{L} e^{1-(\Delta'_{yj}/L)} = 0, \quad j = 1, 2, \ldots, N, \\ \displaystyle\sum_{k=1}^{M} a^*_{ik}\alpha_k + \sum_{k=1}^{M_*} b^*_{ik}\gamma_k - \tau_{\max} A(\Delta^*_{yi}) \sin\left(2\pi \frac{\Delta^*_{xi}}{b}\right) = 0, \quad i = 1, 2, \ldots, M_*, \end{cases} \tag{28}$$

where

$$\begin{cases} a_{ik} = \dfrac{[\cos(k\theta_i) - \cos(k\pi)]}{\sqrt{t_{1i}}}, \\ b_{ik} = \dfrac{T_k(\eta_i) - T_k(\eta_*)}{\sqrt{t_i}}, \\ \theta_i = \dfrac{(i-1)\pi}{M}, \qquad t_{1i} = \tfrac{1}{2}(1 + \cos\theta_i), \\ t_i = \dfrac{R_1}{R_b} t_{1i}, \qquad \eta_i = \dfrac{2(t_i - \rho)}{1-\rho} - 1, \\ \eta_* = -\dfrac{2\rho}{1-\rho} - 1, \end{cases} \tag{29}$$

$$b'_{ik} = \frac{[\cos(k\varphi_i) - \cos(k\pi)]}{\sqrt{t_{2i}}}, \qquad \varphi_i = \frac{(i-1)\pi}{N}, \tag{30}$$

$$\begin{cases} a^*_{ik} = \dfrac{T_k(\eta_{1i}) - \cos k\pi}{\sqrt{t_{1i}}}, \\ b^*_{ik} = \dfrac{-T_k(\eta_*) + \cos k\psi_i}{\sqrt{t_i}}, \\ t_i = \rho + \tfrac{1}{2}(1-\rho)(1 + \cos\psi_i), \qquad \psi_i = \dfrac{(i-1)\pi}{M_*}, \\ t_{1i} = \dfrac{R_b}{R_1} t_i, \qquad \eta_{1i} = 2t_{1i} - 1. \end{cases} \tag{31}$$

Δ_{xi}, Δ_{yi} are the shearing and opening displacements at $x_i = R_1[1 + \cos\theta_i]/2$; $\Delta'_{xj}, \Delta'_{yj}$ are the shearing and opening displacements at $x_j = R_2[1 + \cos\varphi_j]/2$; $\Delta^*_{xj}, \Delta^*_{yj}$ are the shearing and opening displacements at $t_i = \rho + (1-\rho)(1 + \cos\psi_i)/2$.

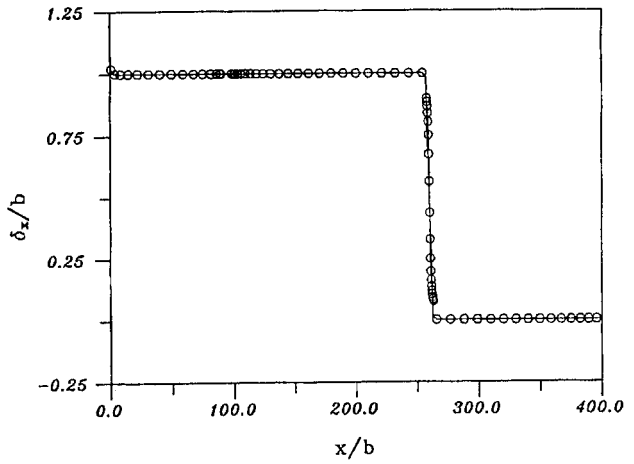

Figure 3. Shear displacement profiles for a pure mode II crack after one dislocation emission for the case of $R_1/b = 90, R_a/b = 100$ and $R_b/b = 420$.

Equation (28) is solved by the Newton-Raphson method. The iterating convergence is guaranteed after five or ten iterations. Most calculations in this paper were carried out with five digits of accuracy for the stress fields in the cohesive zone.

Calculation results

The calculation was carried out with materials parameters $h/b = 1, L/b = 0.2, \tau_0/\mu = 0.01, \sigma_0/E = 0.008, v = 0.3, \tau_{\max}/\mu = 0.159, \sigma_{\max}/E = 0.0766$, and $M = 120, N = 60$ and $M_* = 180$.

Pure shear loading

Figure 3 shows the slip displacement profiles for pure shear loading after one dislocation emission for the case of $R_1/b = 90, R_a/b = 100, R_b/b = 420$, and $K_{II}/\sqrt{2\pi b}\,\tau_0 = 11.6$. The emitted dislocation is located at $x_1/b = 260$. Figure 4 shows the shear stress τ_{xy} distribution ahead of the crack tip.

The slip displacements profiles for pure shear loading after two dislocation emissions for the case of $R_1/b = 113.5, R_a/b = 600, R_b/b = 1000$, and $K_{II}/\sqrt{2\pi b}\,\tau_0 = 12.6$ are shown in Figure 5. The two dislocations are located at $x_1/b = 800$ and $x_2/b = 748$, respectively. The shear stress distributions ahead of the crack tip are shown in Figure 6. The shear stress changes drastically around the center of the emitted dislocation.

Combined tensile and shear loading

The results for a general combined shear and tension loading after emission a single crystal are given in Figures 7 and 8. Figure 7 shows the slip and opening displacement profiles for the case of $R_1/b = 200, R_2/b = 100, R_a/b = 600, R_b/b = 1000, K_I/\sqrt{2\pi b}\,\sigma_0 = 9.69$ and $K_{II}/\sqrt{2\pi b}\,\tau_0 = 10.2$. The stress fields ahead of the crack tip are shown in Figure 8. The shear stress reaches the maximum value at $x/b = 4.8$ and the normal stress reaches the maximum

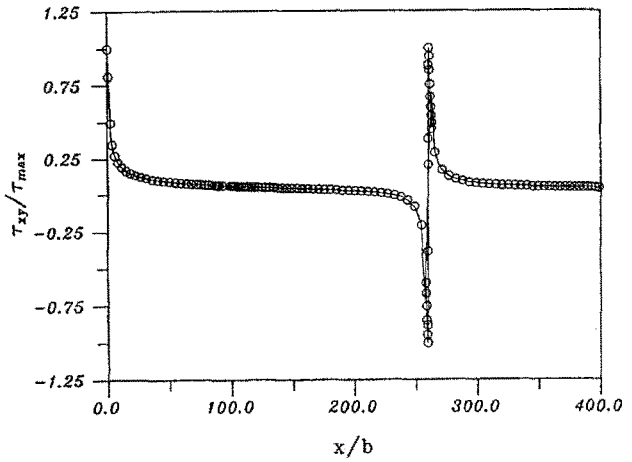

Figure 4. Shear stress distributions ahead of the crack tip after one dislocation emission for the case of $R_1/b = 90$, $R_a/b = 100$ and $R_b/b = 420$.

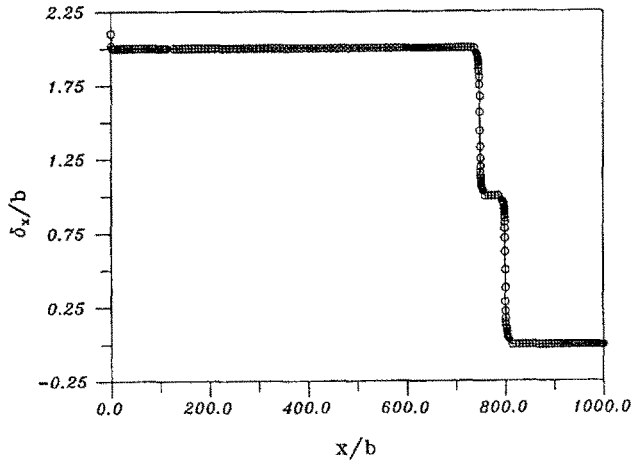

Figure 5. Slip displacement profiles for a pure mode II crack after two dislocation emissions from the crack tip for the case of $R_1/b = 113.5$, $R_a/b = 600$ and $R_b/b = 1000$.

value at $x/b = 4.3$. The shear stress actually vanishes at the crack tip due to the second dislocation being fully nucleated near the crack tip.

5. Dynamical effects

The process of the dislocation emission from the stressed crack tip is actually a dynamic one. The emitted dislocations will rapidly move away from the crack tip area with a high speed.

In this section we give an approximate treatment of the dynamic process of the dislocation emission for the pure shear loading. After a dislocation fully nucleated at the crack tip, the dislocation accelerates very quickly. Through a short distance (about 30–40b), the acceleration tends to zero and the dislocation moves with a nearly constant speed v. We suppose the speed v is below the shear wave speed c_s.

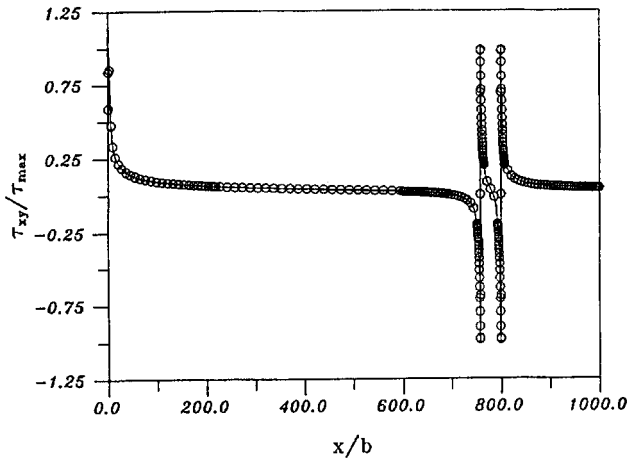

Figure 6. Shear stress distributions along the cohesive zone for a pure mode II crack after two dislocation emissions for the case of $R_1/b = 113.5$, $R_a/b = 600$ and $R_b/b = 1000$.

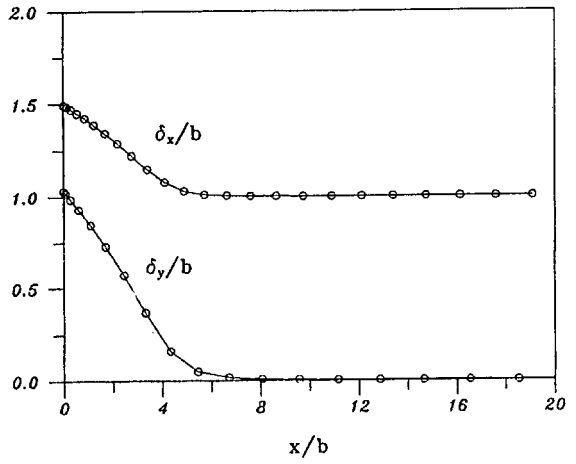

Figure 7. Displacement profiles for a combined mode crack after one dislocation emission from the crack tip for the case of $R_1/b = 200$ and $R_2/b = 100$, $R_a/b = 600$ and $R_b/b = 1000$.

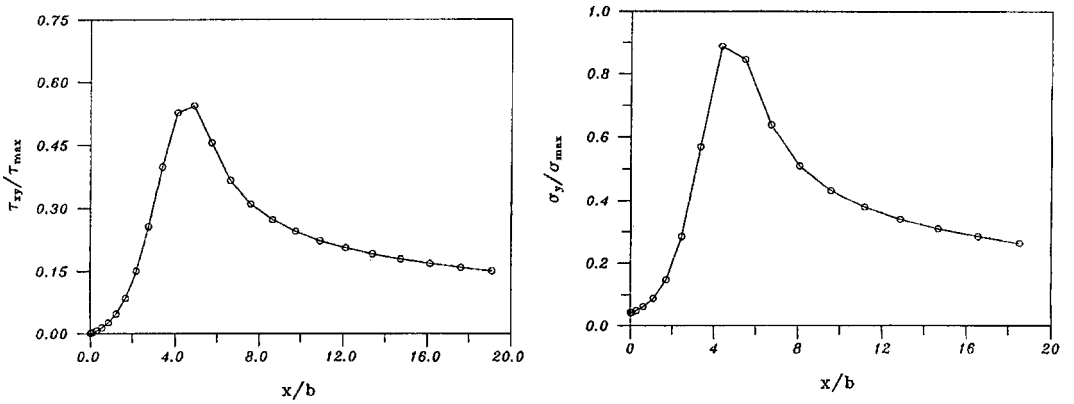

Figure 8. Stress distributions along the cohesive zone for a combined mode crack after dislocation emission for the case of $R_1/b = 200$ and $R_2/b = 100$. $R_a/b = 600$ and $R_b/b = 1000$.

As pointed out by Weertman and Weertman [14], the shear stress produced by an edge dislocation parallel to z-axis and moving uniformly with speed v can be expressed as

$$\tau_{xy} = \frac{2\mu}{(\kappa+1)\pi}\frac{b}{x-x_c}\varepsilon, \tag{32}$$

where x_c is the current position of the moving dislocation, ε the reduction factor

$$\varepsilon = (\kappa+1)\left[\sqrt{1-\omega^2}\sqrt{1-\frac{(\kappa-1)}{(\kappa+1)}\omega^2} - \left(1-\frac{\omega^2}{2}\right)^2\right]\frac{1}{\omega^2}, \tag{33}$$

where $\omega = v/c_s$.

When $v \to 0$, the reduction factor $\varepsilon \to 1$. Hence the influence of the dislocation movement can be characterized by the reduction factor ε.

If we take into account the interaction between the emitted dislocation and the crack faces, the shear stress can be evaluated by the following equation

$$\tau_{xy} = \frac{2\mu}{(\kappa+1)\pi}\sqrt{\frac{x_c}{x}}\frac{b}{(x-x_c)}\varepsilon. \tag{34}$$

Equation (34) is valid only for the steady state which means that the crack tip advances with the same speed v. But in our situation the crack tip does not advance. Therefore (34) only provides an approximate evaluation.

In the cohesive zone, the continuous distributed dislocation ahead of the stationary crack tip can still be treated as the stationary dislocation.

Instead of (8), the basic equation becomes

$$\frac{2\mu}{(\kappa+1)\pi}\left\{\int_0^{R_1}\frac{\sqrt{\tau}\,b_x(\tau)}{x-\tau}\,\mathrm{d}\tau + \frac{\sqrt{x_c}\,b\varepsilon}{(x-x_c)}\right\} = \sqrt{x}(\tau_{xy}-\tau_{xy}^{(0)}). \tag{35}$$

Using the method proposed in Section 4, (35) can easily be solved.

The shear stress distributions along the cohesive zone are plotted in Figure 9 for different moving speeds, with the parameters $R_1/b = 63.5$, and $x_c/b = 200$. The three curves are corresponding to $v/c_s = 0, 0.5$ and 0.9 and $K_{\mathrm{II}}/\sqrt{2\pi b}\,\tau_0 = 10.3, 9.75$ and 8.17, respectively.

The shear stress distribution seems to not be sensitive to the moving speed v of the emitted dislocation. The shear stress distribution actually is controlled by R_1, the length of the cohesive zone, and x_c the current position of the moving dislocation. The external stress intensity factor is equal to $K_{\mathrm{II}}/\sqrt{2\pi b}\,\tau_0 = 7.95$ for the case of $R_1/b = 63.5$ before the dislocation emission. Hence the stress intensity factors $K_{\mathrm{II}}/\sqrt{2\pi b}\,\tau_0$ shielded by the emitted dislocations are 2.35, 1.8 and 0.22, respectively, for the three curves in Figure 9.

Figure 10 shows the stress distribution ahead of the crack tip in a copper crystal for the case of $R_1/b = 30$ and $K_{\mathrm{II}}/\sqrt{2\pi b}\,\tau_0 = 16.0$. In this copper crystal, the crack plane is taken to be the $\{111\}$ plane, crack front is along the $\langle 112\rangle$ direction. Under the mode II loading the partial dislocations will move along $\langle 110\rangle$ direction. Two partial dislocations are combined to form a complete lattice dislocation. The molecular dynamics simulation is carried out on a cracked parallelepiped with a finite boundary by Zhang et al. [17]. Using the molecular dynamics

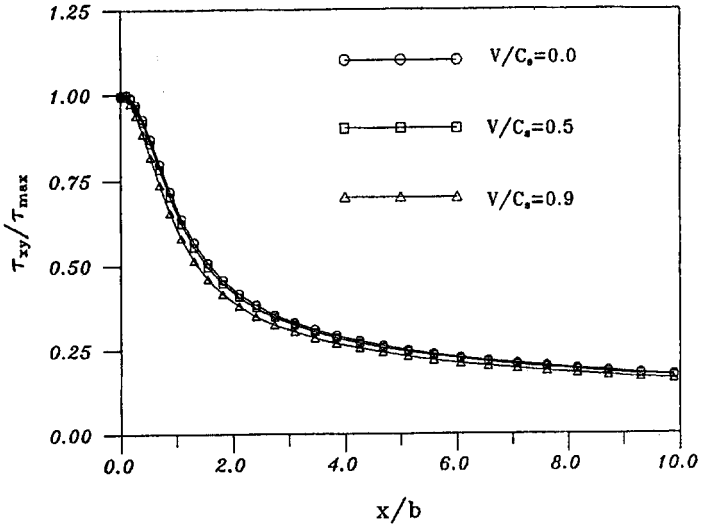

Figure 9. The dynamic effect of the moving speeds of the emitted dislocations on the stress distribution ahead of the crack tip.

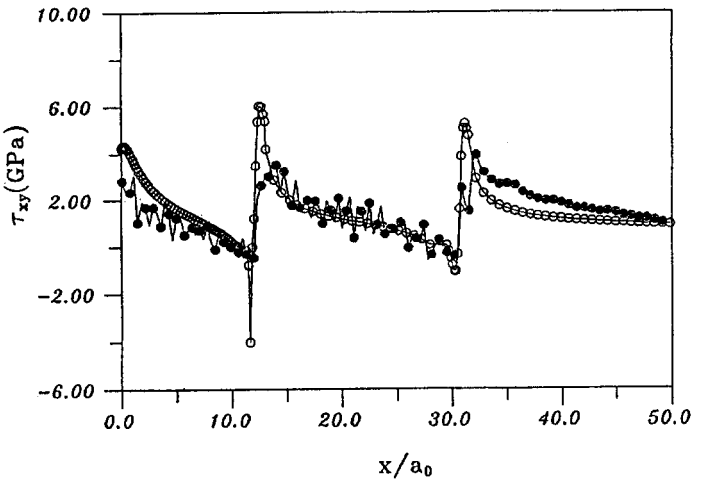

Figure 10. The comparison of the present results (small white circles) and the results (small black circles) of the molecular dynamics simulation for the stress distribution ahead of the crack tip.

simulation, the constitutive relation between the cohesive force and the shear displacement has been calculated, which can be approximately expressed as

$$\tau_x = \tau_{\max} \sin\left(\frac{\pi \Delta_x}{b}\right), \tag{36}$$

where $\tau_{\max} = 4.35\,\text{GPa}$, $b = a_0/(2\sqrt{2})$ and a_0 is lattice parameter.

The shear modulus $\mu = 56.0\,\text{GPa}$. The shear wave speed is $c_s = 2215\,\text{m/s}$. According to the molecular dynamics calculation, two partial dislocations are located at $x_1 = 87b$ and $x_2 = 34b$ and the moving speeds are $v_1 = 1460\,\text{m/s}$ and $v_2 = 1549\,\text{m/s}$, respectively. The molecular dynamics calculation results for the shear stress distribution ahead of the crack tip are also shown in Figure 10. The present results are in good agreement with those of

the molecular dynamics calculation. Very near the crack tip, the present results give higher stresses than those of MD results, because the continuum model is not suitable for this region. Meanwhile near the boundary the present results give lower stresses than those of the MD results since the present results correspond to an infinite plane.

6. Discussion

A unified model for dislocation nucleation, emission and dislocation free zone is proposed in this paper based on the Peierls framework and with a slight modification of the Rice concept. Three regions are identified ahead of the crack tip, that is, the cohesive zone immediately ahead of the crack tip, the plastic zone formed by the emitted dislocations which located out of the crack tip area and a dislocation free zone between those two zones. It is shown by the calculation results that the stress distribution immediately ahead of the crack tip is mainly determined by the parameters R_1, R_2 and the position of the first emitted dislocation x_1. An approximate approach is developed in this paper to analyze the dynamic effects of the dislocation emission. The calculation results indicate that the stresses ahead of the crack tip are not sensitive to the positions and speeds of the emitted dislocations if the emitted dislocations are located far away from the crack tip region. On the other hand, the external stress intensity factors are sensitive to those factors. It should be pointed out that the present analysis concerns only a two-dimensional description, while it is evident that the dislocation emission actually takes place in a three-dimensional geometry by a dislocation loop [15]. The elastic anisotropy and the effect of the thermal activation on the dislocation are also neglected in the present analysis. Further investigation is needed.

Acknowledgements

This research is supported by the Chinese National Natural Science Foundation.

References

1. S. Kobayashi and S.M. Ohr, *Philosophical Magazine* 42 (1980) 763.
2. J.A. Horton and S.M. Ohr, *Scripta Metallurgica* 16 (1982) 621.
3. S.M. Ohr, *Materials Science Engineering* 72 (1985) 1.
4. J.R. Rice and R.M. Thomson, *Philosophical Magazine* 29 (1974) 73.
5. J.R. Rice, *Journal of Mechanics and Physics of Solids* 40 (1992) 239.
6. G. Schoeck, *Philosophical Magazine* 63 (1991) 111.
7. J.M. Rice, G.E. Beltz and Y. Sun, in *Topics in Fracture and Fatigue*, A.S. Argon (ed.), Springer-Verlag (1992) 1.
8. G.E. Beltz and J.R. Rice. In C.L. Terry, D.R. Anthony, P.S. Follansbee, G.S. Daehn (eds.), *Modeling the Deformation of Crystalline Solids* (1991) p. 457.
9. T.C. Wang, *International Journal of Fracture* 69 (1995) 295.
10. R. Thomson, S.J. Zhou, A.E. Carlsson and V.K. Tewary, *Physics Review B* 46 (1992) 10613.
11. R.J. Hill, *Journal of Mechanics and Physics of Solids* 14 (1966) 295.
12. R.J. Asaro, Micromechanics of crystal and polycrystals, *Advances in Applied Mechanics* 23 (1983) 1.
13. K.K. Loo, *Journal of Applied Mechanics* 45 (1978) 797.
14. J. Weertman and J.R. Weertman, Moving dislocation. In F.R. Nabarro (ed.), *Dislocation in Solids*, 3,1. North-Holland (1980).
15. P. Hirth and J. Lothe, *The Theory of Dislocations*. Wiley, New York (1982).
16. F. Erdogan and G.D. Gupta, *Quarterly Applied Mathematics* 1 (1972) 525.
17. Y.W. Zhang, T.C. Wang and Q.H. Tang, *Acta Mechanica Sinica* 11 (1995) 76.